Evidence of a forward energy cascade and Kolmogorov self-similarity in submesoscale ocean surface drifter observations

Andrew C. Poje, Tamay M. Özgökmen, Darek J. Bogucki, and A. D. Kirwan, Jr.

Citation: Phys. Fluids **29**, 020701 (2017); doi: 10.1063/1.4974331
View online: http://dx.doi.org/10.1063/1.4974331
View Table of Contents: http://aip.scitation.org/toc/phf/29/2
Published by the American Institute of Physics

Evidence of a forward energy cascade and Kolmogorov self-similarity in submesoscale ocean surface drifter observations

Andrew C. Poje,[1,a)] Tamay M. Özgökmen,[2] Darek J. Bogucki,[3] and A. D. Kirwan, Jr.[4]
[1]*Department of Mathematics, College of Staten Island, City University of New York, 2800 Victory Boulevard, Staten Island, New York 10314, USA*
[2]*Rosenstiel School of Marine and Atmospheric Science, University of Miami, 4600 Rickenbacker Causeway, Miami, Florida 33149-1098, USA*
[3]*Department of Physical and Environmental Sciences, Texas A&M University, 6300 Ocean Drive, Corpus Christi, Texas 78412-5869, USA*
[4]*School of Marine Science and Policy, University of Delaware, 210 Robinson Hall, Newark, Delaware 19716-3501, USA*

(Received 19 July 2016; accepted 20 September 2016; published online 1 February 2017)

Using two-point velocity and position data from the near-simultaneous release of O(100) GPS-tracked surface drifters in the northern Gulf of Mexico, we examine the applicability of classical turbulent scaling laws to upper ocean velocity fields. The dataset allows direct estimates of both velocity structure functions and the temporal evolution of the distribution of particle pair separations. On 100 m-10 km spatial scales, and time scales of order 1-10 days, all metrics of the observed surface fluctuations are consistent with standard Kolmogorov turbulence theory in an energy cascade inertial-range regime. The sign of the third-order structure function is negative and proportional to the separation distance for scales $\lesssim$10 km where local, fluctuating Rossby numbers are found to be larger than 0.1. The scale-independent energy dissipation rate, or downscale spectral flux, estimated from Kolmogorov's 4/5th law in this regime closely matches nearby microscale dissipation measurements in the near-surface. In contrast, similar statistics derived from a like-sized set of synthetic drifters advected by purely geostrophic altimetric AVISO data agree well with Kolmogorov-Kraichnan scaling for 2D turbulence in the forward enstrophy cascade range. *Published by AIP Publishing.* [http://dx.doi.org/10.1063/1.4974331]

I. INTRODUCTION

As pointed out by Tennekes and Lumley on the very first page of *A First Course in Turbulence*, "Many turbulent flows can be observed easily; watching cumulus clouds or the plume of a smokestack is not time wasted for a student of turbulence."[1] Indeed, the extraordinarily high Reynolds numbers achieved in geophysical flows,[2] either those naturally occurring in clouds or in anthropogenic smokestack plumes, are often cited as ideal testbeds for asymptotic turbulence theories. The first reliable verifications of Kolmogorov's (K41)[3] similarity theory were not from laboratories, but from single-point measurements in tidal channels[4] and the atmospheric boundary layer.[5,6]

The large Reynolds numbers of geophysical flows, however, also present major challenges for universal theories of turbulence. The most obvious is the enormous span of physical processes either directly or indirectly affecting the properties of turbulence observed at a given location at a given time. Time and space scales of ocean flows range from basin-wide circulations and mesoscale eddies dominated by small Rossby and Froude number dynamics, down to microscales where both rotation and stratification effects are negligible. In contrast to the idealized picture of turbulence as the downscale cascade of energy input at some distinct "large-scale," spectrally distant from the scale where this energy is frictionally dissipated as heat, energy input (and extraction) mechanisms in geophysical flows span the entire spectrum. The forcing is unsteady, episodic, and spatially inhomogeneous. Spectrally, the picture might be something like Lumley's "leaky," non-equilibrium cascade,[7] complicated by the presence of numerous source and sink terms and the fact that the basic direction of the spectral transfer is itself scale dependent. Important complications also arise from the modulation and feedback between the turbulence and many geophysical wave phenomena spanning a similarly broad range of scales.

Assuming, for the moment, that the primary energy source for ocean currents occurs at the planetary scale,[8] global energy flux equilibrium requires that this energy input be balanced by viscous dissipation at the smallest scales of motion. In the ocean, such scales are $\mathcal{O}$(1 cm) or less. Gyre-scale circulations spawn energetic fields of mesoscale eddies (spatial scale 10's of kilometers, time scales of weeks). At these scales, motions are strongly constrained by rotation and stratification. The dynamics, well described by the quasi-geostrophic turbulence theory, is classically characterized by the inverse cascade of energy from the injection scale towards larger scales. If mesoscales cannot contribute directly to the forward, downscale energy cascade, there must exist alternate transfer routes for maintaining the global budget.

a)Email: andrew.poje@csi.cuny.edu

The characteristics of the turbulence, and the processes driving it, in the regime connecting mesoscales (with presumed upscale energy transfer) and classical microscale turbulence (with well-known downscale energy transfer) are not entirely well-established. High resolution satellite imagery now regularly provides snapshots of the rich structure of this intermediate, so-called submesoscale range; roughly motions with spatial scales 100 m–10 km, and time scales of hours to days. Submesoscale turbulence, at least as viewed through the lens of its effects on the surface stirring of scalar fields, is "observed easily" in high-resolution (1 km) images of ocean color.[9] These scales, where the dynamics is no longer entirely dominated by vanishing Rossby and Froude numbers, mark the instability transition from the predominantly two-dimensional mesoscale to the more familiar, fully three-dimensional turbulent microscale. Given their potential role in providing a pathway for global energy transfer and their dominant role in the local transport of bio-geochemical tracers, the dynamics of submesoscale processes has become a subject of much recent research.[10–18]

Spectral estimates in the upper submesoscale range, derived from the amalgamation of repeated commercial ship transects of the Gulf Stream (the oceanic equivalent of atmospheric MOZAIC commercial plane data[19]) indicate the persistence of a relatively shallow slope ($E(k) \sim k^{-\beta}, \beta \leq 2$) at scales well below the main deformation radius.[20] Similar spectral results, extending down to ≈1 km wavelengths, were obtained for much shorter averaging times by novel two-point, two-ship velocity measurements.[21] Analysis of the submesoscale tracer-variance cascade in the same region clearly indicates the importance of local stirring by ageostrophic motions with energy at length-scales smaller than 100 m.[22] Model studies, upon which much of our present understanding of the submesocales is based, consistently show strong scaling behavior of the kinetic energy spectra with spectral slope $\beta \approx 2$ extending to ever-finer scales as the spatial resolution increases[11] and process models have begun to explicitly address dynamic pathways from balanced QG motions to ageostrophic cascades.[17,18] However, while remote sensing images of the effects of submesoscale stirring are now readily available, synoptic *in situ* measurements of the underlying velocity field are still rare. The submesoscales represent an "awkward" spatio-temporal range for current observational techniques.[8] The spatial scales are unduly large and the temporal scales similarly short for single ships to traverse without encountering severe aliasing issues. Moored arrays are typically too expensive to provide the spatial sampling needed for synoptic observations at these scales.

Difficulties associated with simultaneously measuring a broad range of spatial scales over an extended spatial region can be circumvented by Lagrangian-based observations, provided that large enough numbers of instruments are released at a given time.[23] This is especially true at the ocean surface where relatively inexpensive, GPS-tracked surface drifters can be deployed to report accurate real-time position information. Lagrangian based observational strategies have long been a staple for oceanographic measurements.[24] Standard connections between classical turbulence theory[25,26] and Lagrangian-based observations have been used to estimate velocity scaling laws in the ocean and atmosphere.[27,28] Contrary to the exponential pair separation expected for 2D turbulence in the enstrophy cascade regime, drifter-based investigations targeted at the submesoscales have found Richardson scaling, indicative of a shallow spectral slope of the underlying velocity field, extending well into the submesoscale separation regime in a variety of settings.[29–31]

Here we consider data from a particularly large surface drifter deployment conducted in July 2012. The GLAD (Grand LAgrangian Deployment) observational program took place in the DeSoto Canyon region of the northern Gulf of Mexico. Funded by the Gulf of Mexico Research Initiative in response to the DeepWater Horizon spill of 2010, the primary goal of the experiment was to measure, using GPS-tracked surface drifters, the statistical structure of surface currents at the submesoscale. The experiment was specifically designed to determine whether the relative dispersion of dense clusters of simultaneously launched drifters was driven by local processes acting at pair separation scales or, instead, nonlocally stirred by the strain field imposed by larger mesoscale structures.

The primary goal here is to investigate, in light of the building evidence listed above, to what extent classical turbulence laws extend into the submesoscale. Previous analysis, presented in terms of second-order structure functions and scale dependent diffusivity estimates,[32] indicates general agreement between the GLAD observations and simple scaling law predictions for turbulence in an energy cascade inertial-range. Second-order structure functions are consistent with K41, $k^{-5/3}$, spectra and scale dependent diffusivities match Richardson's $r^{4/3}$ law. While the data are consistent with energy cascade scaling, the existing metrics provide no information on the direction of the cascade process. Here we re-examine a subset of the GLAD database in terms of standard turbulence self-similarity measures including higher order structure functions and, via Kolmogorov's 4/5th law, attempt to determine the direction of the cascade in a scale-dependent manner.

The drifter data and available information about the local ocean state, including potentially representative observations of the local turbulence microstructure are presented in Sec. II. Section III presents results on the absolute and relative dispersion statistics from the Lagrangian data. In Section IV we discuss two-point velocity statistics. Here we establish the direction of the energy cascade obtained from Lagrangian observations at submesoscales and the degree of ocean surface compressibility. The paper concludes with a summary and brief discussion of the analysis.

II. LAGRANGIAN OBSERVATIONAL PROGRAM: GLAD

During GLAD, approximately 300 standard CODE surface drifters[33,34] were released over a two week period. CODE drifters are designed to follow currents in the upper 1 m with 1-3 cm/s velocity errors for wind speeds up to 10 m/s. The drifters were equipped with GPS units reporting 5-10 m accurate position information every 5 min. As detailed in Yaremchuk and Coelho,[35] quality control was conducted via acceleration-filtering and non-causal spline interpolation

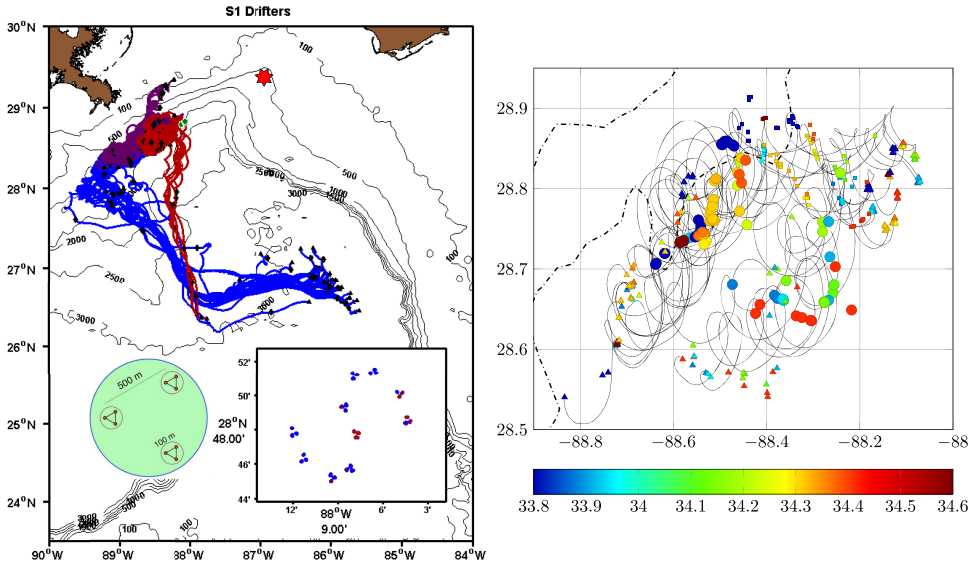

FIG. 1. (a) Overview of GLAD S1 deployment, centered at (88.15 W, 28.8 N), showing 28 day trajectories. Insets show S-shaped initial launch pattern of 10, 9 drifter nodes and the nested triangle arrangement of 9 drifters in each node. The large red star marks the location where microstructure dissipation measurements were made. (b) Selected 8 day trajectories and locations of the 86 drifters from the launch. Daily drifter positions (symbols) are color coded by sea-surface salinity from CTD casts at launch locations. Dotted-dashed lines show 500 and 1000 m isobath contours.

was used to produce trajectory and velocity information at uniformly sampled 15 min intervals.

GLAD consisted of four directed, near-simultaneous launches of 20 or more drifters.[36] Here we concentrate on the initial *S*1 launch of 90 drifters conducted in the western region of the DeSoto Canyon on July 22, 2012. Details of the launch template and resulting 28 day trajectories are shown in Fig. 1(a). The launch template, 10 nodes (labeled A-J, with A furthest west) of 9 drifters each, was designed to (a) allow rapid deployment of the overall $\sim 8 \times 12$ km *S* pattern while (b) maximizing pair statistics at small (100 m and 500 m) initial separations (see insets). The total deployment was completed in 6 h with 86 of the 90 drifters reporting for the initial 12 day period we consider here. As shown in Fig. 1(b), during this time the 86 drifter cluster remained relatively coherent, drifting southwest roughly along the bathymetry without indications of significant large-scale shear. The daily positions of each of the 86 drifters are shown, colored by the near surface salinity measured at each node. For clarity, only select trajectories (one for each 100 m triplet) are plotted. As expected for shallow summer mixed layers, individual trajectories are dominated by wind driven inertial oscillations. Daily positions show both a tendency for frontal alignment and significant mixing of the initial surface salinity signals.

The structure of the upper ocean density field in the region was measured along-track by a fixed-depth, shipborne flow-through salinity-temperature system[36] with vertical profiles obtained at each of the 3, 100 m triplet locations in each node via hand-held CTD casts. Temperature and salinity profiles at 3 of the 10 nodes are shown in Fig. 2. The data indicate the presence of small, shallow fronts of cold-fresh water above warm-salty water with 10-15 m mixed layer showing strong compensation of the unstable surface temperature by salinity. There is considerable variation in profiles both between nodes (horizontal spacing ≈3 km) and also within nodes ($\Delta x = 500\,m$) as well as evidence of strong temperature mixing/overturning at the mixed layer base. While shallow mixed layer depths typically argue for considerably weaker submesoscale energies in summer, in the western DeSoto, a location subjected to the presence of Mississippi outflow, density structures with small horizontal scales exist. The net importance of these smaller scale density-driven currents on the observed structure of the near-surface velocity field is likely enhanced by the fact that, at least over the duration of the GLAD experiment, this region remained far removed from straining by mesoscale features associated with the loop current.

Although no direct turbulence microstructure measurements were made in the course of the *S*1 drifter launch, vertical kinetic energy dissipation profiles were obtained 5 days later. A single cast of a vertical microstructure profiler (VMP) was conducted on 27th July at the northern tip of the DeSoto Canyon, 122 km NE from the S1 deployment (location marked

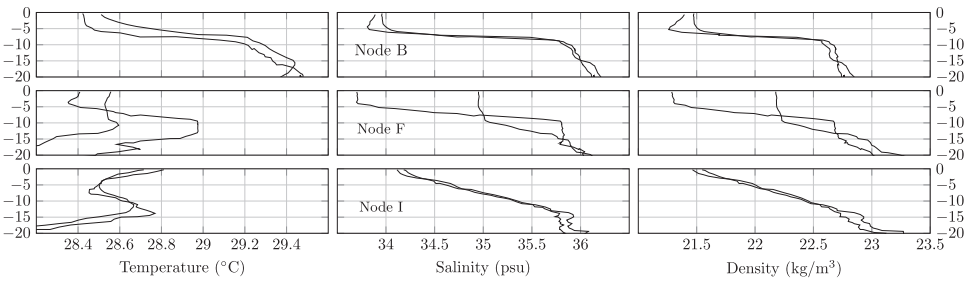

FIG. 2. Vertical profiles of temperature (left) and salinity (center) and density (right) as measured by small boat CTD casts at selected GLAD S1 launch nodes. Unstable surface temperature signals strongly compensated by salinity.

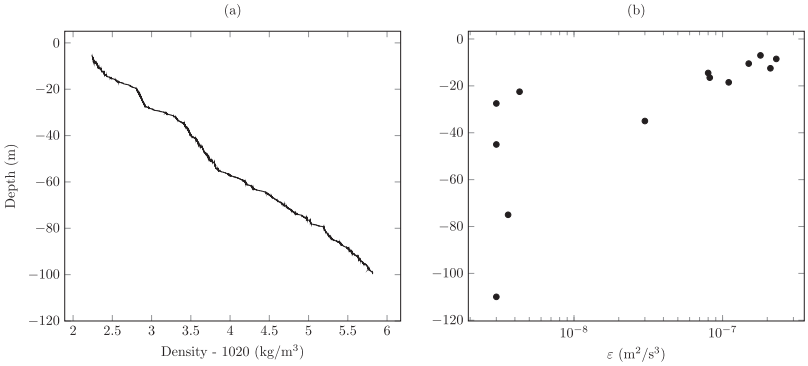

FIG. 3. (a) Density profile at the location of microstructure measurements on July 27. (b) Vertical profile of observed microstructure TKE dissipation at same location.

by star on Fig. 1(a)). Stratification profiles at this site were similar to those observed in the western canyon, with salinity compensated density and mixed layer depths at around 20 m. The density profile at this location on 27th July, Fig. 3(a), indicates a weakly stratified 15 m deep layer with a more stratified layer at 15 m–20 m depth. Consistent with observations during the initial period following the $S1$ deployment, background swell during the VMP was characterized by wave amplitudes <0.25 m.

Turbulence properties were measured using a Rockland VMP250 (Victoria, Canada) microstructure loose-tethered free-fall profiler with dual shear sensors[37] enabling estimation of the turbulent energy dissipation rate (ε) using standard techniques. VMP250 collected time series of horizontal velocity shear. The vertical profile of the shear was binned over varying depths and at least 1.5 m long (corresponding to time series at least 3 s long) were converted to velocity shear power spectra. The noise contamination due to acceleration was removed using a Goodman coherent noise removal algorithm.[38] Under usual assumptions of homogeneity and isotropy, values of ε were then derived by integrating the velocity shear power spectrum, $\Psi(k)$, in wave number space following the method of Ref. 37. The power spectra of velocity shear is given by

$$\varepsilon = \frac{15}{2}\nu\overline{\left(\frac{\partial u}{\partial z}\right)^2} = \frac{15}{2}\nu\int_{k_{\min}}^{k_{\max}}\Psi(k)dk, \qquad (1)$$

where u denotes horizontal velocity, ν is the kinematic viscosity, and k is the wavenumber. When the profile exhibited large (>5°) inclination angles, measurements were discarded. The results are presented in Fig. 3(b).

The derived ε is characterized by elevated value 2×10^{-7} m^2/s^3 between the closest to the surface VMP bin at 7-12 m depth. Within the mixed layer, the dissipation decreases montonically below 15 m depth, more rapidly below 20 m. The dissipation attains its deep water value of 2×10^{-9} m^2/s^3 just below the mixed layer and is then characterized by a relatively low, constant value, down to the deepest measurements taken at 120 m.

In the absence of surface or internal wave breaking, the main source of upper ocean energy dissipation is attributed to the wind stress[39] such that the turbulent kinetic energy input into the ocean varies as $\propto W_{10}^3$, where W_{10} is the wind speed at 10 m above the sea surface. Month long *in situ* observations indicate that more than 70% of the total wind stress related energy dissipation takes place within the mixed layer.[40]

Wind speeds on July 27 had decreased from 7 m/s a few hours prior to the VMP deployment to around 2.5 m/s during the VMP deployment. The mean wind speed between the $S1$ launch and VMP deployments (i.e., between days 204.5 and 209.5) was ≈5 m/s. Thus, we expect that the VMP observed dissipation represents a lower bound on mixed layer dissipation between days 204.5 and 209.5. Since the mean wind speed was around 5 m/s during the analyzed time, the corresponding dissipation should then be 8× larger, $\approx 10^{-6}$ m^2/s^3, corresponding to doubled wind speeds. We have some experimental indication that dissipation level, i.e., $\approx 10^{-6}$ m^2/s^3 likely represents the upper bound on dissipation during the analyzed time period. Observation of Ref. 41 yielded dissipation values of $\approx 10^{-6}$ m^2/s^3 in a near surface 2 m thick layer during the strongest wind speed (7.5 m/s) encountered. Thus we expect mean day-time, wind driven dissipation in the near-surface layer to be well estimated at $\mathcal{O}(10^{-7})$ m^2/s^3.

III. SELF-SIMILARITY IN LAGRANGIAN STATISTICS

Absolute and relative dispersion statistics for the $N = 86$ drifters are shown in Fig. 4. The absolute dispersion is ballistic initially with

$$A^2(t) = \frac{1}{N}\sum_{i=1}^{N}(\mathbf{x}_i(t) - \mathbf{x}_i(0))^2 = \langle(\mathbf{x}(t) - \mathbf{x}(0))^2\rangle = v_0^2 t^2, \quad (2)$$

for at least the first 12 h. The estimated energy, $v_0^2 = 0.19$ m^2/s^2, was significantly smaller in the western canyon region than in other GLAD launches, consistent with the observed slow drift of the $S1$ cluster.

Fig. 4(b) shows the evolution of the adjusted relative dispersion computed from 86 drifter pairs with initial separation less than 300 m. Errors bars show 95% confidence intervals obtained by standard boot-strapping on 10 000 subsamples. After a short interval of slower growth (nominally matching Batchelor's quadratic regime[42]), Richardson scaling holds over a narrow range of intermediate times (2-8) days. The existence of this regime is indicated by the short plateau in the Richardson compensated curve shown in the inset. The estimated slope, C_R, in the Richardson regime,

$$\langle(r(t) - r(0))^2\rangle = C_R t^3, \qquad (3)$$

is $\mathcal{O}(10^{-9})$ m^2/s^3.

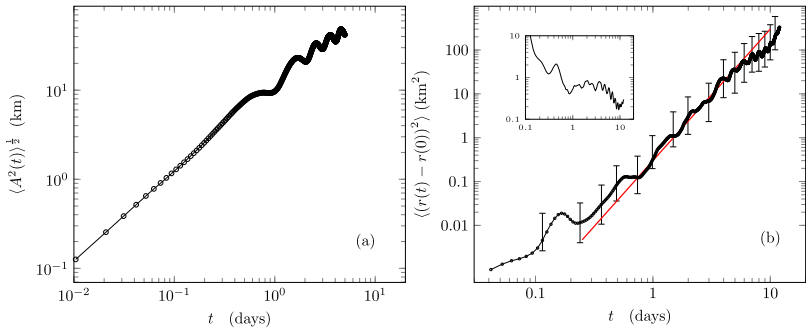

FIG. 4. (a) RMS absolute dispersion of drifters over the first 8 days. (b) Relative dispersion over the first 12 days. Error bars show 95% confidence levels computed from bootstrapping on 10 000 subsamples. Solid line indicates Richardson, $D^2 \sim t^3$, scaling. The inset shows Richardson compensated results, $\frac{\langle (r(t)-r(0))^2 \rangle}{t^3}$, with units 10^{-9} m^2/s^3.

While Richardson's $r^2 \sim t^3$ scaling for the relative dispersion is dimensionally consistent with Kolmogorov energy cascade arguments, similar power-law behavior can be observed in purely kinematic velocity fields[43,44] and does not directly imply the presence (or direction) of a dynamic cascade. The existence of an inertial range does imply that Lagrangian statistics at such scales should show temporal self-similarity. Additional evidence of Lagrangian self-similarity in the surface drifter data is shown in Fig. 5. First, we consider the backwards in time correlation function of pair separations,

$$R(t,\tau) = \langle r(t) r(t+\tau) \rangle, \tag{4}$$

where $-t \le \tau \le 0$ and the average is taken over all pairs. As originally argued by Richardson, even in a statistically stationary turbulence, the rate at which pairs separate is a time-dependent process and the separation at any time depends on the cumulative history of the individual trajectories. The correlation time of pairs grows as time increases. However, in a Kolmogorov inertial range, the only physical time scale is time itself and one expects self-similar behavior for $R(t,\tau)$ for rescaled delay times, τ/t. Fig. 5(a) indicates a reasonable collapse of the data to a single dimensionless function, $g(t/\tau)$, for times consistent with those where Richardson scaling is observed. The persistence time of the correlations during this period is roughly estimated (solid line) to be $\tau = t/3$ indicating that particle pairs remember, at any time, a considerable fraction of their previous history.

Additionally, we consider the second order Lagrangian structure function,

$$S_l^2(\tau,0) = \langle ||\mathbf{v}(\tau) - \mathbf{v}(0)||^2 \rangle, \tag{5}$$

with the average taken over all trajectories. Assuming the existence of an energy cascading inertial range with cascade rate ε, standard Kolmogorov dimensional analysis implies that

$$S_l^2(\tau,0) = C_0 \varepsilon \tau. \tag{6}$$

Fig. 5(b) shows the results for the drifter data plotted in terms of ε using the value $C_0 = 6.5$ estimated from experiments and simulations of three-dimensional turbulence.[45,46] The results clearly indicate the presence of near-inertial modes and, as is typical for all investigations of Lagrangian structure functions, display only a modest plateau of inertial range scaling since increasing time lags eventually lead to super-inertial range separation scales. Notably, however, a plateau does exist at time lags corresponding to 1-10 km spatial separations (Fig. 4(a)). Although Eq. (6) is only a dimensional relationship and C_0 known to be Reynolds number dependent,[45] the order of magnitude of the resulting dissipation rate estimate from the drifter data is consistent with near-surface microstructure measurements.

IV. TWO-POINT VELOCITY STATISTICS

The GLAD deployment strategy was explicitly designed to maximize statistical sampling, at least initially, of a broad range of particle pair separation scales. In order to infer information on the spatial structure of the surface flow, we will treat the drifter velocity observations as Eulerian measurements, albeit on a time evolving, highly non-uniform spatial grid. The resulting Eulerian estimates are certainly influenced by the non-uniform sampling of the flow by the surface constrained drifters, especially in the presence of significant surface convergence. Nonetheless, the observations provide a uniquely large dataset of two-point ocean velocity observations with which to test standard turbulence scaling laws at 100 m–10 km, submesoscale, separations.

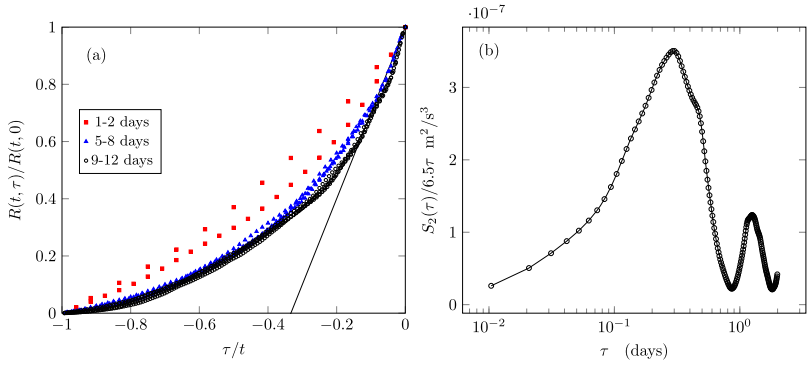

FIG. 5. (a) Self similar collapse backward-in-time correlation of pair separation distances, $R(t,\tau)$ on the similarity variable, $s = t/\tau$. (b) Second order Lagrangian structure function scaled by 6.5τ.

Scale dependent, two-point velocity statistics were obtained from the 86 drifter database by first calculating the full relative dispersion matrix,

$$D_{ij}(t) = \text{dist}\left(\mathbf{x}_i(t) - \mathbf{x}_j(t)\right), \tag{7}$$

for all times $t \leq 12$ days. Assuming homogeneity and isotropy, standard longitudinal and transverse velocity increments, defined by

$$\begin{aligned} \Delta u_l(r,t) &= (\mathbf{u}(\mathbf{x}+\mathbf{r},t) - \mathbf{u}(\mathbf{x},t)) \cdot \frac{\mathbf{r}}{||\mathbf{r}||}, \\ \Delta u_t(r,t) &= (\mathbf{u}(\mathbf{x}+\mathbf{r},t) - \mathbf{u}(\mathbf{x},t)) \times \frac{\mathbf{r}}{||\mathbf{r}||}, \end{aligned} \tag{8}$$

were also calculated at each time for each pair. Statistics were obtained by time-averages over the data conditioned on binned separation distances.

In order to both assess the ability of the available drifter data-density to test predicted scaling behavior and to highlight contributions from ageostrophic components of the surface velocity field, we also make use of synthetic drifters advected by the geostrophic velocities derived from AVISO satellite altimetry of the region over the same time interval. As detailed in Olascoaga *et al.*[47] and Berta *et al.*,[48] the available AVISO data are meshed at 1°/10° resolution with temporal updates every 24 h. The 90 synthetic drifters were launched on the original GLAD *S*1 template at the closest available time to the actual launch.

Fig. 6 shows probability distributions of two-point longitudinal velocity increments for the drifter data and the synthetic trajectories from AVISO fields conditioned on separation distance. Both the small-scale ($r \leq 1$ km, top) and larger scale (5 km $\leq r \leq$ 10 km, bottom) plots show data for three sub-bins of separation distances indicated in the caption. For each sub-bin, the distributions are normalized by their standard deviation. Best fit Gaussian curves are indicated by dashed-lines. For sub-kilometer separation scales, both the observations and geostrophic AVISO data exhibit Gaussian cores with highly non-Gaussian tails. Unlike the nearly symmetric AVISO results, the small-scale GLAD data are clearly negatively skewed. At larger separation scales, consistent with the spatial resolution of the altimetric fields, the geostrophic AVISO data are nearly Gaussian while the drifter observations show persistent negative skewness.

A. Structure functions and scaling

The *n*th order structure functions are calculated from moments of the velocity increment distribution via

$$S^n_\alpha(r) = \langle \Delta u^n_\alpha \rangle, \tag{9}$$

where the greek index denotes either the longitudinal or transverse component.

Standard K41 scaling for inertial range, three-dimensional turbulence, where the local time scale is set by the (forward) energy cascade rate ε, implies that

$$S^n_\alpha(r) = C_n(\varepsilon r)^{n/3}. \tag{10}$$

In contrast, for two-dimensional turbulence in the enstrophy cascade range where the time scale is set by the enstrophy cascade rate ν, the scaling exponent is unity and

$$S^n_\alpha(r) = \tilde{C}_n \nu^{n/3} r^n. \tag{11}$$

Scaling of the second order longitudinal structure function for drifter and AVISO-based data is shown in Fig. 7(a). As expected for spatial scales well below the radius of deformation, the geostrophic AVISO data show excellent agreement with r^2 enstrophy cascade scaling. This is an indication (at least for the non-local dispersion induced by coarse-grained AVISO altimetry) that the available Lagrangian data density

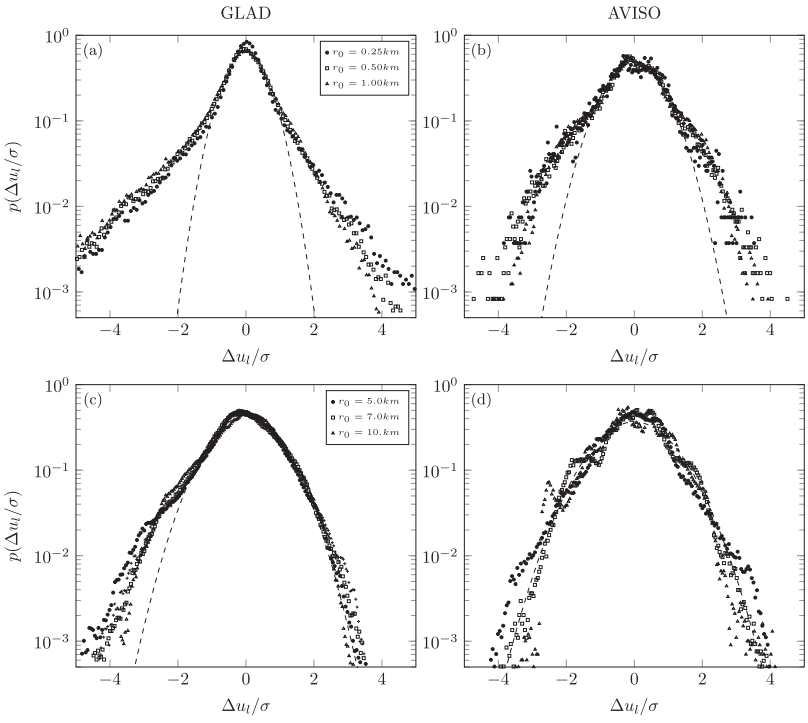

FIG. 6. Probability distributions of longitudinal velocity increments from GLAD observations (a) and (c) and synthetic trajectories advected by AVISO-based geostrophic velocities (b) and (d). (a) and (b) each show results for small separation distances (bins centered at r = 0.25, 0.5, and 1 km). (c) and (d) show results for larger separations (bins centered at r = 5, 7, and 10 km).

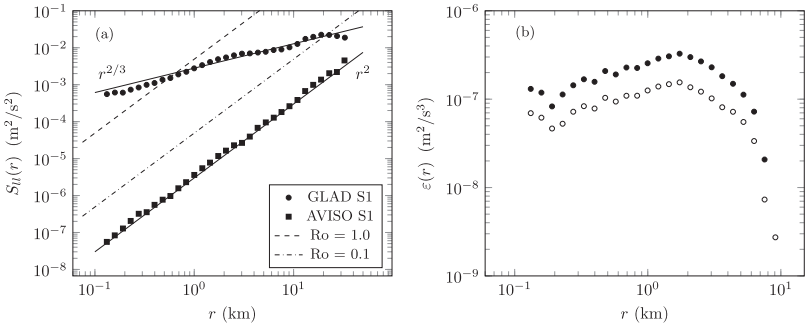

FIG. 7. (a) Second order longitudinal structure function versus separation distance showing Richardson-Kolmogorov, $r^{2/3}$, energy cascade scaling for GLAD data and Kraichnan, r^2, enstrophy cascade scaling for AVISO-based synthetic trajectories. (b) Sign-reversed third order longitudinal structure function scaled by r for the GLAD observations.

is high enough and that inhomogeneity and anisotropy are not large enough to significantly effect observations of expected scaling laws. In contrast, the actual drifter observations indicate a scaling exponent much lower than 2 and much closer to the 2/3 prediction consistent with energy cascade arguments. Best fit exponent over the range 100 m $\leq r \leq$ 10 km is 0.70 $\pm$ 0.05.

A coarse estimate of the direct effects of rotation on the fluctuations can be established by defining a local, fluctuating Rossby number by

$$\mathrm{Ro}^2(r) = \frac{\Delta u_l^2(r)}{f^2 r^2}.$$

With f set to 7×10^{-5} s^{-1}, comparisons of $\Delta u_l^2(r) = (\mathrm{Ro}fr)^2$ for Ro = 0.1 and 1 to observations indicate that the local Rossby number estimated from the drifter data remains greater than 0.1 for separation scales smaller than $\approx$10 km. The distinct differences in scaling exponents of the structure functions and the relatively large value of the local Rossby number in the observations indicate the importance of ageostrophic velocity components at these scales.

B. Direction of cascade

The energy-cascade scaling for even-order structure functions (along with Richardson's law for two-point dispersion) supplies no information about the direction of the spectral energy-cascade and identical results are obtained in both standard three-dimensional inertial ranges and in the inverse-cascade range for 2D turbulence.[49] Odd-order structure functions, however, do determine the cascade direction. Kolmogorov's 4/5th law,

$$\langle \Delta u_l^3(r)\rangle = -\frac{4}{5}\varepsilon r, \tag{12}$$

directly relates the dissipation rate (and its sign) to the third order structure function. Without recourse to unknown scaling constants or simple dimensional analysis, the relationship serves as one of the few "exact" results of turbulence theory.

The 4/5th law can be generalized to any dimension,[50] d,

$$\langle \Delta u_l^3(r)\rangle = -\frac{12}{d(d+2)}\varepsilon r, \tag{13}$$

with the sign of ε negative for an inverse, upscale cascade. An alternate form, derived using typical geophysical scaling arguments applicable to mesoscale atmospheric flows, has been derived by Lindborg and Cho,[51]

$$\langle \Delta u_l^3(r)\rangle + \langle \Delta u_l(r)\Delta u_t^2(r)\rangle = -2\varepsilon r, \tag{14}$$

which includes both the third order longitudinal structure function and the mixed longitudinal-traverse statistic and is consistent with alternate 2D forms.[52]

The scale dependence of the third order structure functions calculated from the drifter data, plotted in terms of the energy dissipation rate, is given in Fig. 7(b). Solid circles show the dissipation estimated directly from the 4/5th law while open circles are the results from Eq. (14). The data, in both cases, indicate a scale-independent, positive value of ε across the submesoscale range. At separation scales $\gtrsim$10 km, roughly where the local Rossby number is less than 0.1, the sign changes from positive to negative. The magnitude, in units of W/kg, is $\mathcal{O}(10^{-7})$ again consistent with the observed upper ocean microstructure dissipation estimates.

In contrast, data from the synthetic AVISO-based drifters agree remarkably well with enstrophy cascade scaling for structure functions up to fourth order. Fig. 8 shows comparisons of the structure functions for the GLAD drifters (panels (a) and (c)) and the synthetic AVISO trajectories (panels (b) and (d)) plotted under energy-cascade scaling (top panels) and enstrophy-cascade scaling (bottom panels). As shown in panel (a), the drifter observations scale reasonably well with $r^{p/3}$ across the observed range of scales. Given the limited 12 day extent of the sample, and the observed dispersion rate, data densities for $r >$ 20 km are low. As shown in panel (d), the AVISO data, especially for the even-order structure functions, demonstrate even clearer scaling with enstrophy-cascade exponent, $r^{1/p}$.

C. Surface compressibility

In terms of the given measures, the observed drifter data are notably consistent with standard K41 inertial range scaling behavior for 3D turbulence, including the existence of a scale independent, positive spectral energy flux towards smaller scales. The observed dissipation rate, computed at 100 m–10 km scales, is also remarkably similar to direct measurements of the "true" micro-scale dissipation rate in the near-surface ocean in this region at this time. The surface-constrained drifters, however, only provide information on the two-dimensional, divergent horizontal surface velocity field making any explicit connection between the drifter derived estimates of dissipation and the direct microstructure measurements speculative at best.

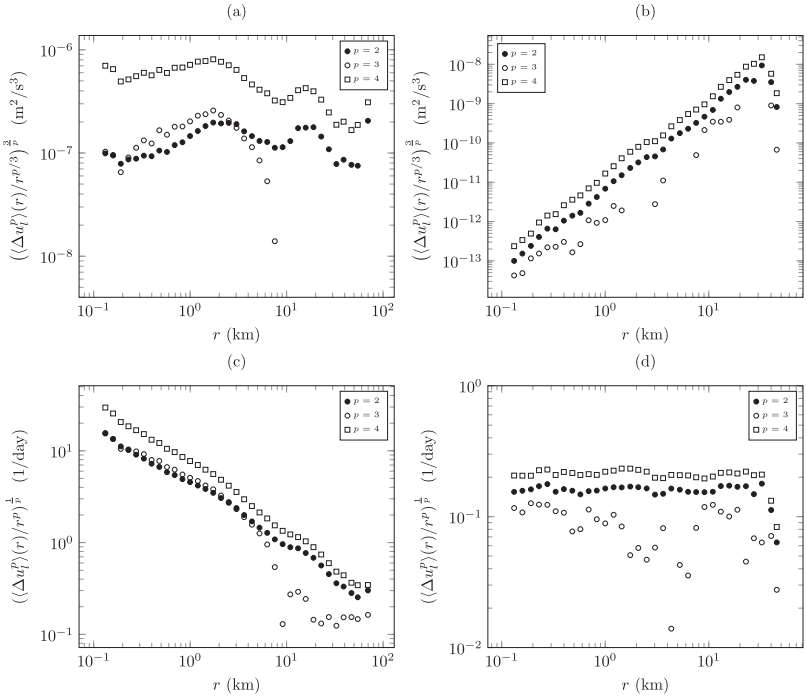

FIG. 8. (a) Structure functions from GLAD observations scaled by energy cascade rate. Note that $p = 3$ is sign-reversed, consistent with a forward energy cascade. (b) Structure functions AVISO-based data scaled by energy cascade parameters. (c) Structure functions from GLAD observations scaled by enstrophy cascade rate. (d) Same as (c) for AVISO-based trajectories.

There is, in addition, a distinct mismatch between the apparent Richardson scaling of the simple relative dispersion results shown in Fig. 4(b) and the 4/5th law dissipation estimates of Fig. 7(b). From the inset of Fig. 4(b), the slope of the relative dispersion curve in the nominal Richardson regime is $\mathcal{O}(10^{-9})$ m^2/s^3. Using the Obukhov-Richardson relation,

$$r^2 = g\varepsilon t^3 \tag{15}$$

with a dissipation estimate of $\varepsilon \approx 10^{-7}$ m^2/s^3 implies a Richardson constant, $g \approx 10^{-2}$, approximately two orders of magnitude smaller than the usual 3D value of 0.55, and smaller still than the 2D value of 3.8. If we accept the drifter-derived dissipation estimate, then the observed surface dispersion is significantly slower than expected. Alternatively, the observations indicate that the efficiency of the fluctuating surface velocity field in dispersing particles (the effective horizontal eddy-diffusivity) is far lower than is typically found in incompressible flows. As shown in Poje *et al.*[36] for the same data set, a similar ($\mathcal{O}(10^{-2})$) difference is found when comparing the diffusivity computed from direct observations of the drifter cluster to scale dependent diffusivities estimated from the second-order structure function.

One plausible explanation for the apparent reduction in pair dispersion for a given level of fluctuating energy is a high degree of horizontal convergence in the surface velocity field. Experiments and computations on compressible surface turbulence indicate energy cascade scaling of the surface velocity structure functions, but a reduction of the Richardson dispersion exponent itself from 3 to roughly 1.5 due to strong particle clustering in convergence zones.[53]

The degree of compressibility in the observations can be assessed by examining the relative values of the second-order longitudinal and transverse structure functions. Standard von Karman-Howarth analysis[54] for a homogeneous, isotropic incompressible field gives

$$S_{tt}(r) = S_{ll}(r) + \frac{r}{2}\frac{dS_{ll}}{dr}, \tag{16}$$

where S_{tt} and S_{ll} denote the second order transverse and longitudinal functions. For any positive power law scaling of the longitudinal structure function, incompressibility implies that $S_{tt} > S_{ll}$.

Recently, Helmholtz decompositions on second order statistics have been proposed as a means of analyzing the scale-dependence of the rotational and divergent contributions to the horizontal kinetic energy spectra in the available ship and airplane track velocity measurements.[55,56] Following Lindborg,[56] the total second order structure function can be written either in standard form or in terms of the incompressible, rotational component, S_{rr}, and the horizontally divergent contribution from the velocity potential, S_{dd}, as

$$S_{ll} + S_{tt} = S_{rr} + S_{dd}.$$

The rotational and divergent components can be recovered from

$$S_{rr} = S_{tt} + \int_0^r \frac{1}{r}(S_{tt} - S_{ll})\,dr,$$
$$S_{dd} = S_{tt} - \int_0^r \frac{1}{r}(S_{tt} - S_{ll})\,dr. \tag{17}$$

This decomposition for the drifter observations is shown in Fig. 9 where the integral contribution from missing data in the interval 0 m $< r \lesssim$ 100 m has been neglected. The results, with $S_{tt} \leq S_{ll}$ over all scales, are clearly inconsistent with 2D incompressibility. Fig. 9(b) indicates that contributions from the divergent component are roughly twice as large as the rotational.

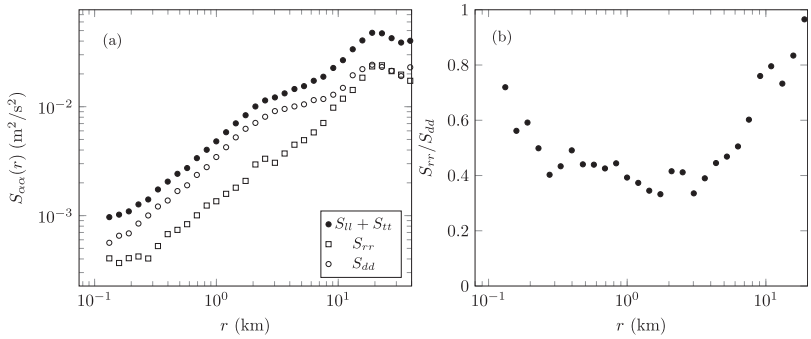

FIG. 9. (a) Decomposition of second order structure functions into rotational and divergent components. (b) Ratio of rotational to divergent contributions.

V. CONCLUSIONS

Two-point velocity and position observations provided by the simultaneous launch of 86 near-surface drifters were used to compute statistics over the submesoscale separation range. The primary goal was to determine whether, and how well, standard, inertial-range turbulence scaling arguments apply to the observed velocity fluctuations at scales which are intermediate between the largely 2D, geostrophic mesoscale and the fully 3D microscale. For the given dataset, the results are remarkably consistent with Kolmogorov, forward energy cascade inertial range scaling.

Notably, the observed third order structure function is negative for separation lengths where the fluctuating Rossby number is appreciable and scales remarkably well with separation distance in this range. The order of magnitude estimate for the scale independent dissipation rate provided by the 4/5th law closely matches the near surface microstructure measurements shown in Fig. 3 taken in the same region. For comparison, similar statistics derived from a like-sized set of synthetic drifters advected by purely geostrophic altimetric AVISO data agree well with Kolmogorov-Kraichnan scaling for 2D turbulence in the forward enstrophy cascade range. Helmholtz decomposition of the second-order structure function indicates that the surface velocity field observed by the drifters is far from 2D incompressible. The presence of strong surface convergence zones is a candidate mechanism for explaining the anomalously slow growth of the observed relative dispersion for the given level of fluctuating kinetic energy.

The observations are consistent with a decidedly ageostrophic, forward cascade of energy from scales where the fluctuations are not entirely dominated by rotation. While the drifter-derived estimates of the dissipation rate at 100 m horizontal separations match surface microstructure measurements, the existence of an inertial-range directly linking submesoscales to the fully 3D microscale remains unknown. At such scales, the upper ocean contains a host of distinct processes and features, either driven directly by a forward, downscale energy flux from larger scales or directly forced at their own scale by the atmosphere. These include the Langmuir turbulence,[57–62] arising from the direct interaction of wind and surface waves, surface wave Stokes drift, and direct wind forcing of the near-surface current. Convective plumes are strongly modulated by the diurnal cycle and wind forcing also influences material dispersion at the surface.[63] Frontal density structures, with sub-kilometer scales, exhibiting highly salinity compensated density profiles clearly play a role in the observations and the *S*1 launch was unique in this regard. Perhaps not surprisingly, the dynamics in the ocean surface velocity field are inhomogeneous even over the confines of the DeSoto Canyon region. Analysis of other GLAD launches shows even-order structure functions, $S^p(r)$, scaling with $r^{p/2}$ over submesoscale separations.

ACKNOWLEDGMENTS

This research paper was made possible by a grant from the Gulf of Mexico Research Initiative. We acknowledge additional support under Grant No. N00014-11-1-0087 from the Office of Naval Research for MURI OCEAN 3D+1. Data are publicly available through the Gulf of Mexico Research Initiative Information and Data Cooperative (GRIIDC) at https://data.gulfresearchinitiative.org/data/R1.x134.073:0004, doi:10.7266/N7VD6WC8.

This paper is dedicated to Professor J. L. Lumley.

[1] H. Tennekes and J. Lumley, *A First Course in Turbulence* (MIT Press, 1972).
[2] As pointed out by Grant *et al.*,[4] the Reynolds number in the observed tidal channel flow, 3×10^8, is more than an order of magnitude larger than that of an interstellar gas cloud 100 light years in diameter moving at 10 km/s.
[3] A. Kolmogorov, "The local structure of turbulence in incompressible viscous fluid for very large Reynolds numbers," Proc.: Math. Phys. Sci. **434**, 9–13 (1991).
[4] H. Grant, R. Stewart, and A. Moilliet, "Turbulence spectra from a tidal channel," J. Fluid Mech. **12**, 241 (1962).
[5] F. R. Payne and J. L. Lumley, "One-dimensional spectra derived from an airborne hot-wire anemometer," Q. J. R. Meteorol. Soc. **92**, 397–401 (1966).
[6] C. Sheih, H. Tennekes, and J. Lumley, "Airborne hot-wire measurements of small-scale structure of atmospheric turbulence," Phys. Fluids **14**, 201 (1971).
[7] J. L. Lumley, "Some comments on turbulence," Phys. Fluids A **4**, 203–211 (1992).
[8] J. McWilliams, "Submesoscale currents in the ocean," Proc. R. Soc. A **472**, 20160117 (2016).
[9] See https://oceancolor.gsfc.nasa.gov for images.
[10] L. Thomas, A. Tandon, and A. Mahadevan, "Submesoscale processes and dynamics," Geophys. Monogr. **177**, 17–38 (2008).
[11] X. Capet, J. C. McWilliams, M. J. Molemaker, and A. F. Shchepetkin, "Mesoscale to submesoscale transition in the California current system. Part I: Flow structure, eddy flux, and observational tests," J. Phys. Oceanogr. **38**, 29–43 (2008).
[12] B. Fox-Kemper, R. Ferrari, and R. W. Hallberg, "Parameterization of mixed layer eddies. Part I: Theory and diagnosis," J. Phys. Oceanogr. **38**, 1145–1165 (2008).
[13] P. Klein and G. Lapeyre, "The oceanic vertical pump induced by mesoscale and submesoscale turbulence," Annu. Rev. Mar. Sci. **1**, 351–375 (2009).
[14] J. R. Taylor and R. Ferrari, "Buoyancy and wind-driven convection at mixed layer density fronts," J. Phys. Oceanogr. **40**, 1222–1242 (2010).
[15] A. Mahadevan, A. Tandon, and R. Ferrari, "Rapid changes in mixed layer stratification driven by submesoscale instabilities and winds," J. Geophys. Res.: Oceans **115**, C03017, doi:10.1029/2008jc005203 (2010).

[16]Y. Zhong, A. Bracco, and T. Villareal, "Pattern formation at the ocean surface: Sargassum distribution and the role of the eddy field," Limnol. Oceanogr.: Fluids Environ. **2**, 12–27 (2012).
[17]R. Barkan, K. Winters, and S. Llewellyn Smith, "Energy cascades and loss of balance in a reentrant channel forced by wind stress and buoyancy fluxes," J. Phys. Oceanogr. **45**, 272–293 (2015).
[18]N. Brüggemann and C. Eden, "Routes to dissipation under different dynamical conditions," J. Phys. Oceanogr. **45**, 2149–2168 (2015).
[19]E. Lindborg, "Can the atmospheric kinetic energy spectrum be explained by two-dimensional turbulence?," J. Fluid Mech. **388**, 259–288 (1999).
[20]J. Callies and R. Ferrari, "Interpreting energy and tracer spectra of upper-ocean turbulence in the submesoscale range (1-200 km)," J. Phys. Oceanogr. **43**, 2456–2474 (2013).
[21]A. Y. Shcherbina, E. A. D'Asaro, C. M. Lee, J. M. Klymak, M. J. Molemaker, and J. C. McWilliams, "Statistics of vertical vorticity, divergence, and strain in a developed submesoscale turbulence field," Geophys. Res. Lett. **40**, 4706–4711, doi:10.1002/grl.50919 (2013).
[22]E. Kunze, J. Klymak, R.-C. Lien, R. Ferrari, C. Lee, M. Sundermeyer, and L. Goodman, "Submesoscale water-mass spectra in the Sargasso Sea," J. Phys. Oceanogr. **45**, 1325–1338 (2015).
[23]T. Özgökmen, A. Poje, and P. Fischer, "On multi-scale dispersion under the influence of surface mixed layer instabilities and deep flows," Ocean Modell. **56**, 16–30 (2012).
[24]T. Rossby, "Evolution of Lagrangian methods in oceanography," in *Lagrangian Analysis and Prediction of Coastal and Ocean Dynamics*, edited by A. Griffa, A. D. Kirwan, A. Mariano, T. Özgökmen, and T. Rossby (Cambridge University Press, 2007), pp. 1–38.
[25]L. F. Richardson, "Atmospheric diffusion shown on a distance-neighbour graph," Proc. R. Soc. A **110**, 709–737 (1926).
[26]A. Okubo, "Horizontal dispersion of floatable particles in vicinity of velocity singularities such as convergences," Deep-Sea Res. Oceanogr. Abstr. **17**, 445 (1970).
[27]A. F. Bennett, "A Lagrangian analysis of turbulent diffusion," Rev. Geophys. **25**, 799–822, doi:10.1029/RG025i004p00799 (1987).
[28]J. LaCasce, "Statistics from Lagrangian observations," Prog. Oceanogr. **77**, 1–29 (2008).
[29]R. Lumpkin and S. Elipot, "Surface drifter pair spreading in the North Atlantic," J. Geophys. Res.: Oceans **115**, C12017, doi:10.1029/2010jc006338 (2010).
[30]K. Schroeder, J. Chiggiato, A. C. Haza, A. Griffa, T. M. Özgökmen, P. Zanasca, A. Molcard, M. Borghini, P. M. Poulain, R. Gerin, E. Zambianchi, P. Falco, and C. Trees, "Targeted Lagrangian sampling of submesoscale dispersion at a coastal frontal zone," Geophys. Res. Lett. **39**, L11608, doi:10.1029/2012GL051879 (2012).
[31]S. Berti, F. D. Santos, G. Lacorata, and A. Vulpiani, "Lagrangian drifter dispersion in the southwestern Atlantic Ocean," J. Phys. Oceanogr. **41**, 1659–1672 (2011).
[32]A. C. Poje, T. M. Özgökmen, J. B. Lipphart, B. Haus, E. H. Ryan, A. C. Haza, G. Jacobs, A. J. H. M. Reniers, J. Olascoaga, G. Novelli, A. Griffa, F. J. Beron-Vera, S. Chen, P. Hogan, E. Coelho, J. A. D. Kirwan, H. Huntley, and A. J. Mariano, "The nature of surface dispersion near the Deepwater Horizon oil spill," Proc. Natl. Acad. Sci. U. S. A. **111**, 12693–12698 (2014).
[33]R. E. Davis, "Drifter observations of coastal surface currents during CODE: The method and descriptive view," J. Geophys. Res.: Oceans **90**, 4741–4755, doi:10.1029/JC090iC03p04741 (1985).
[34]P. Poulain, R. Gerin, E. Mauri, and R. Pennel, "Wind effects on drogued and undrogued drifters in the Eastern Mediterranean," J. Atmos. Oceanic Technol. **26**, 1144–1156 (2009).
[35]M. Yaremchuk and E. Coelho, "Filtering drifter trajectories sampled at submesoscale resolution," IEEE J. Oceanic Eng. **40**, 497–505 (2014).
[36]A. C. Poje, T. M. Özgökmen, B. L. Lipphardt, B. K. Haus, E. H. Ryan, A. C. Haza, G. A. Jacobs, A. J. H. M. Reniers, M. J. Olascoaga, G. Novelli, A. Griffa, F. J. Beron-Vera, S. S. Chen, E. Coelho, P. J. Hogan, A. D. Kirwan, H. S. Huntley, and A. J. Mariano, "Submesoscale dispersion in the vicinity of the Deepwater Horizon spill," Proc. Natl. Acad. Sci. U. S. A. **111**, 12693–12698 (2014).
[37]R. G. Lueck, F. Wolk, and H. Yamazaki, "Oceanic velocity microstructure measurements in the 20th century," J. Oceanogr. **58**, 153–174 (2002).
[38]L. Goodman, E. R. Levine, and R. G. Lueck, "On measuring the terms of the turbulent kinetic energy budget from an AUV," J. Atmos. Oceanic Technol. **23**, 977–990 (2006).
[39]P. A. Hwang and M. A. Sletten, "Energy dissipation of wind-generated waves and whitecap coverage," J. Geophys. Res.: Oceans **113**, C02012, doi:10.1029/2007jc004277 (2008).
[40]A. Wüest, G. Piepke, and D. C. Van Senden, "Turbulent kinetic energy balance as a tool for estimating vertical diffusivity in wind-forced stratified waters," Limnol. Oceanogr. **45**, 1388–1400 (2000).
[41]D. J. Bogucki, K. Huguenard, B. K. Haus, T. M. Ozgokmen, A. Reniers, and N. J. M. Laxague, "Scaling laws for the upper ocean temperature dissipation rate," Geophys. Res. Lett. **42**, 839–846, doi:10.1002/2014GL062235 (2015).
[42]G. Batchelor, "Diffusion in a field of homogeneous turbulence: II. The relative motion of particles," Math. Proc. Cambridge Philos. Soc. **48**, 345–362 (1952).
[43]F. C. G. A. Nicolleau and A. F. Nowakowski, "Presence of a Richardson's regime in kinematic simulations," Phys. Rev. E **83**, 056317 (2011).
[44]G. L. Eyink and D. Benveniste, "Suppression of particle dispersion by sweeping effects in synthetic turbulence," Phys. Rev. E **87**, 023011 (2013).
[45]L. Biferale, E. Bodenschatz, M. Cencini, A. Lanotte, N. Ouellette, F. Toschi, and H. Xu, "Lagrangian structure functions in turbulence: A quantitative comparison between experiment and direct numerical simulation," Phys. Fluids **20**, 065103 (2008).
[46]B. L. Sawford and P. K. Yeung, "Kolmogorov similarity scaling for one-particle Lagrangian statistics," Phys. Fluids **23**, 091704 (2011).
[47]M. J. Olascoaga, F. J. Beron-Vera, G. Haller, J. Trianes, M. Iskandarani, E. F. Coelho, B. K. Haus, H. S. Huntley, G. Jacobs, A. D. Kirwan, B. L. Lipphardt, T. M. Özgökmen, A. J. H. M. Reniers, and A. Valle-Levinson, "Drifter motion in the Gulf of Mexico constrained by altimetric Lagrangian coherent structures," Geophys. Res. Lett. **40**, 6171–6175, doi:10.1002/2013gl058624 (2013).
[48]M. Berta, A. Griffa, M. G. Magaldi, T. M. Özgökmen, A. C. Poje, A. C. Haza, and M. Josefina Olascoaga, "Improved surface velocity and trajectory estimates in the Gulf of Mexico from blended satellite altimetry and drifter data," J. Atmos. Oceanic Technol. **32**, 1880–1901 (2015).
[49]M. Jullien, J. Paret, and P. Tabeling, "Richardson pair dispersion in two-dimensional turbulence," Phys. Rev. Lett. **82**, 2872–2875 (1999).
[50]G. Falkovich, K. Gawdzki, and M. Vergassola, "Particles and fields in fluid turbulence," Rev. Mod. Phys. **73**, 913–975 (2001).
[51]E. Lindborg and J. Cho, "Horizontal velocity structure functions in the upper troposphere and lower stratosphere 2. Theoretical considerations," J. Geophys. Res.: Atmos. **106**, 10233–10241, doi:10.1029/2000JD900815 (2001).
[52]G. Eyink, "Local 4/5-law and energy dissipation anomaly in turbulence," Nonlinearity **16**, 137–145 (2003).
[53]J. Cressman, J. Davoudi, W. Goldburg, and J. Schumacher, "Eulerian and Lagrangian studies in surface flow turbulence," New J. Phys. **6**, 53 (2004), see Ref. 24.
[54]U. Frisch and A. N. Kolmogorov, *Turbulence: The Legacy of A. N. Kolmogorov* (Cambridge University Press, 1995).
[55]O. Buhler, J. Callies, and R. Ferrari, "Wave-vortex decomposition of one-dimensional ship-track data," J. Fluid Mech. **756**, 1007–1026 (2014).
[56]E. Lindborg, "A Helmholtz decomposition of structure functions and spectra calculated from aircraft data," J. Fluid Mech. **762**, R4 (2014).
[57]S. Leibovich and A. Tandon, "Three-dimensional Langmuir circulation instability in a stratified layer," J. Geophys. Res. **98**, 16501, doi:10.1029/93JC01234 (1993).
[58]E. Skyllingstad and D. Denbo, "An ocean large-eddy simulation of Langmuir circulations and convection in the surface mixed layer," J. Geophys. Res.: Oceans **100**, 8501–8522, doi:10.1029/94JC03202 (1995).
[59]E. A. D'Asaro, "Turbulent vertical kinetic energy in the ocean mixed layer," J. Phys. Oceanogr. **31**, 3530–3537(2001).
[60]T. Kukulka, A. J. Plueddemann, J. H. Trowbridge, and P. P. Sullivan, "Rapid mixed layer deepening by the combination of Langmuir and shear instabilities: A case study," J. Phys. Oceanogr. **40**, 2381–2400 (2010).
[61]S. E. Belcher, A. L. M. Grant, K. E. Hanley, B. Fox-Kemper, L. Van Roeke, P. P. Sullivan, W. G. Large, A. Brown, A. Hines, D. Calvert, A. Rutgersson, H. Pettersson, J. R. Bidlot, P. A. E. M. Janssen, and J. A. Polton, "A global perspective on Langmuir turbulence in the ocean surface boundary layer," Geophys. Res. Lett. **39**, L18605, doi:10.1029/2012GL052932 (2012).
[62]E. A. D'Asaro, J. Thomson, A. Y. Shcherbina, R. R. Harcourt, M. F. Cronin, M. A. Hemer, and B. Fox-Kemper, "Quantifying upper ocean turbulence driven by surface waves," Geophys. Res. Lett. **41**, 102–107, doi:10.1002/2013gl058193 (2014).
[63]J. Mensa, T. Özgökmen, A. Poje, and J. Imberger, "Material transport in a convective surface mixed layer under weak wind forcing," Ocean Modell. **96**, 226–242 (2015).